The perfectly matched layer for the ultra weak variational formulation of the 3D Helmholtz equation

Tomi Huttunen[1,*] Jari P. Kaipio[1] and Peter Monk[2]

[1] *Department of Applied Physics, University of Kuopio, P.O.Box 1627, 70211 Kuopio, Finland*

[2] *Department of Mathematical Sciences, University of Delaware, Newark, DE 19716*

SUMMARY

We investigate the feasibility of using the perfectly matched layer (PML) as an absorbing boundary condition for the ultra weak variational formulation (UWVF) of the 3D Helmholtz equation. The PML is derived using complex stretching of the spatial variables. This leads to a modified Helmholtz equation for which the UWVF can be derived. In the standard discrete UWVF, the approximating subspace is constructed from local solutions of the Helmholtz equation. In previous studies plane wave basis functions have been advocated because they simplify the building of the UWVF matrices. For the PML domain we propose a special set of plane wave basis functions which allow fast computations and efficiently reduce spurious numerical reflections.

The method is validated by numerical experiments. In comparison to a low order absorbing boundary condition, the PML shows superior performance.

KEY WORDS: Perfectly matched layer, ultra weak variational formulation, acoustic scattering, wave

*Correspondence to: Department of Applied Physics, University of Kuopio, P.O.Box 1627 70211 Kuopio, Finland

Contract/grant sponsor: Work of Tomi Huttunen and Jari P. Kaipio has been supported by Finnish Academy grants 44042, 54065, 72431, 80773 and 200627. Work of Tomi Huttunen has been supported by grants from Jenny and Antti Wihuri Foundation and Finnish Cultural Foundation of Northern Savo. Research of Peter Monk is supported by a grant from US AFOSR.

propagation, Helmholtz equation

1. Introduction

The ultra weak variational formulation (UWVF) has been proposed as a promising alternative to finite element methods for large-scale wave propagation and scattering problems. In the UWVF, a priori information about the solution is included in the approximation subspace. Therefore, it may reduce the computational burden associated with wave problems at high wave number.

Originally, Cessenat and Després applied the UWVF method to the Helmholtz and Maxwell equations [7, 6] in 2D and 3D, respectively. Furthermore, the UWVF for the Helmholtz problem in an inhomogeneous media was derived in [6] while no numerical experiments were performed. Subsequently, numerical results for inhomogeneous medium in 2D were given in [21]. Recently, the UWVF method has been extended also to 2D elastic wave problems [20].

The UWVF relies on the decomposition of the original wave problem into set of subproblems which are connected via impedance-like boundary conditions. For the geometric partitioning of the problem, the method can utilize a standard finite element mesh provided the material parameters in each element are homogeneous. Including a priori information of the local solutions of the problem and using suitable integration by parts, the UWVF can be derived as a variational problem over element interfaces. Moreover, by discretizing the UWVF with properly chosen plane wave basis functions, the resulting UWVF integrals can be computed in a closed form which makes the assembly of appropriate matrices very fast.

In many applications, it is essential to replace a physically unbounded wave problem by a bounded one and to use an absorbing boundary condition (ABC) to restrict spurious numerical reflections from the artificial exterior boundary. In general, exact absorbing boundary conditions are non-local and therefore, involve large computational effort. To simplify computations, various approximate schemes has been studied [15]. Traditionally, absorbing boundary conditions are approximated with local differential operators (see. e.g [12] or [19]).

Low order operators are simple to implement but do not necessary give an acceptable accuracy, unless the artificial boundary is far from the scatterer [22]. General drawbacks of accurate high order differential operators are their limitation to certain boundary geometries and that they perfectly annihilate waves only in certain incident directions [19].

Partly due to the special treatment of the boundary conditions in the UWVF scheme, only low order absorbing boundary conditions have been used to truncate the computational domain with this method. Their implementation is straightforward but in many cases, they lack sufficient numerical accuracy. Higher order ABCs might improve accuracy but those have not been yet developed for the UWVF method. An alternative to high order ABCs for reducing the boundary reflections is the perfectly matched layer (PML).

In [3] Bérenger proposed a computational damping layer, namely the perfectly matched layer, which surrounds the actual computational domain and efficiently absorbs waves from the computational domain. Originally, the PML was developed for Maxwell's equations but it has also been extended to problems generated by the Helmholtz equation [17, 24]. The PML has been used successfully with the finite difference and finite element methods. An attractive property of the PML is its applicability to very general geometries. A drawback is that the damping layer increases the size of the computational domain and therefore, the number of degrees of freedom in the problem.

In this study, the PML is applied as an absorbing boundary condition for UWVF computations. Since the approximating subspace for the UWVF is chosen utilizing information on local solutions of the problem, it is vital to understand how the PML changes the original equation to be solved. We analyze the PML for the inhomogeneous Helmholtz equation and derive the PML equations using the change of variables method. This approach is due to [8] and has been applied previously for example in [9, 10]. The idea of the PML is to add a *complex stretching* function to spatial variables. This leads to a modified Helmholtz equation for which the UWVF can be derived. Furthermore, plane wave solutions for the Helmholtz-PML equation can be used as basis function for the discrete UWVF.

It is known from previous studies with the finite difference method that the damping coefficient in the PML must increase at least linearly inside the layer to obtain satisfactory

results. A higher order increase has been shown to further reduce the spurious reflections [3]. We show that in the UWVF scheme, even a low order constant PML gives accuracy sufficient for most engineering applications.

This article is organized as follows. Section 2 discusses the derivation of the PML using the change of variables approach. The ultra weak variational formulation for the modified Helmholtz equation is derived in Section 3. Finally, we present three dimensional numerical simulations in Section 4, and in Section 5 we discuss the results and draw some conclusions.

2. Derivation of the PML using a change of variables

We consider the inhomogeneous Helmholtz equation

$$\nabla \cdot \left(\frac{1}{\rho}\nabla\right) u + \frac{\kappa^2}{\rho} u = f \tag{1}$$

with spatially variable density $\rho = \rho(r)$ and wave number $\kappa = \kappa(r)$. The wave number is defined as $\kappa(r) = \omega/c(r) + i\alpha(r)$ where ω is the angular frequency, $c(r)$ the speed of sound and $\alpha(r)$ absorption coefficient. To allow us to apply the UWVF, we assume that both κ and ρ are piecewise constant.

Let us utilize the change variables scheme and introduce a complex stretching of the spatial variables $r(x, y, z) = (x, y, z)$ given by

$$x' = \begin{cases} x + \dfrac{i}{\kappa}\displaystyle\int_{x_0}^{x} \sigma_{0,x}(|x| - x_0)^n dx, & |x| \geq x_0, \\ x, & |x| < x_0, \end{cases} \tag{2}$$

$$y' = \begin{cases} y + \dfrac{i}{\kappa}\displaystyle\int_{y_0}^{y} \sigma_{0,y}(|y| - y_0)^n dy, & |y| \geq y_0, \\ y, & |y| < y_0, \end{cases} \tag{3}$$

$$z' = \begin{cases} z + \dfrac{i}{\kappa}\displaystyle\int_{z_0}^{z} \sigma_{0,z}(|z| - z_0)^n dz, & |z| \geq z_0, \\ z, & |z| < z_0. \end{cases} \tag{4}$$

In addition, we define $r' = (x', y', z')$.

To simplify notation we also define

$$\sigma_\xi(\xi) = \sigma_{0,\xi}(|\xi| - \xi_0)^n, \qquad \xi = x, y, z \tag{5}$$

where $\sigma_{0,\xi}$ is a constant and n is an integer. Moreover, let us define

$$d_x(x) = \begin{cases} 1 + \dfrac{i}{\kappa}\sigma_x(x), & |x| \geq x_0, \\ 1, & |x| < x_0, \end{cases} \tag{6}$$

$$d_y(y) = \begin{cases} 1 + \dfrac{i}{\kappa}\sigma_y(y), & |y| \geq y_0, \\ 1, & |y| < y_0, \end{cases} \tag{7}$$

$$d_z(z) = \begin{cases} 1 + \dfrac{i}{\kappa}\sigma_z(z), & |z| \geq z_0, \\ 1, & |z| < z_0. \end{cases} \tag{8}$$

Now we observe that the derivative of the stretched variable x' is

$$\frac{\partial x'}{\partial x} = d_x(x) \tag{9}$$

with similar expressions for $\frac{\partial y'}{\partial y}$ and $\frac{\partial z'}{\partial z}$. This allows a straightforward substitution

$$\frac{\partial}{\partial x} \to \frac{\partial}{\partial x'} = \frac{1}{d_x}\frac{\partial}{\partial x}. \tag{10}$$

To simplify notation, we have omitted the explicit spatial dependence of d_x, d_y and d_x from here on. We can then rewrite the Helmholtz equation in stretched variables as

$$\frac{1}{d_x}\frac{\partial}{\partial x}\left(\frac{1}{d_x\rho}\frac{\partial u}{\partial x}\right) + \frac{1}{d_y}\frac{\partial}{\partial y}\left(\frac{1}{d_y\rho}\frac{\partial u}{\partial y}\right) + \frac{1}{d_z}\frac{\partial}{\partial z}\left(\frac{1}{d_z\rho}\frac{\partial u}{\partial z}\right) + \frac{\kappa^2}{\rho}u = f. \tag{11}$$

In a more compact form Equation (11) can be written as

$$\nabla \cdot \left(\frac{1}{\rho}A\nabla u\right) + \frac{\kappa^2\eta^2}{\rho}u = f\eta^2. \tag{12}$$

where $\eta^2 = d_x d_y d_z$ and

$$\mathrm{diag}(A) = \left(\frac{d_y d_z}{d_x}, \frac{d_x d_z}{d_y}, \frac{d_x d_y}{d_z}\right) \tag{13}$$

It is obvious that the standard inhomogeneous Helmholtz equation (1) is obtained from (12) by choosing $\eta = 1$ and $A = I$ where I is the identity matrix. Or, in other words, Equation (1) follows if one chooses $x' = x$, $y' = y$ and $z' = z$. Therefore, to simplify following discussion we do not distinguish PML and non-PML regions. Instead, we present our study using the more general equation (12).

3. The ultra weak variational formulation for the Helmholtz-PML equation

In this section we outline the ultra weak variational formulation for the Helmholtz-PML equation (12). In this study, the matrix A and parameter η are obtained via the complex stretching of the spatial variables. Since a thorough derivation of the UWVF for the inhomogeneous Helmholtz problems has been given in [6], we present only a short review omitting the details.

Let us first partition the domain Ω into disjoint elements $\{\Omega_k\}_{k=1}^K$. We assume that the mesh is chosen such that the parameters ρ and κ are constant on each element and define $\rho_k \equiv \rho|_{\Omega_k}$ and $\kappa_k \equiv \kappa|_{\Omega_k}$. For two elements Ω_k and Ω_j we define $\Sigma_{kj} = \partial\Omega_k \cap \partial\Omega_j$ with normal pointing from Ω_k into Ω_j if $\Sigma_{kj} \neq \emptyset$. A face of Ω_k on the exterior boundary is denoted by $\Gamma_k = \Gamma \cap \partial\Omega_k$ with unit outward normal ν_k.

[Figure 1 about here.]

In this study, tetrahedral finite elements are used for partitioning. Although the UWVF method itself is not limited to any special element shape, this choice has been made due to abundance of tetrahedral finite element mesh generators. Use of other types of elements is possible but this topic is not studied here.

For the UWVF scheme, we decompose the Helmholtz equation (12) into subproblems for each element Ω_k, $k = 1, \cdots, K$ and define a collection of coupled problems as

$$\nabla \cdot \left(\frac{1}{\rho_k} A_k \nabla u_k \right) + \frac{\kappa_k^2 \eta_k^2}{\rho_k} u_k = f \eta_k^2 \qquad \text{in } \Omega_k, \tag{14}$$

$$u_k = u_j \qquad \text{on } \Sigma_{kj}, \tag{15}$$

$$\frac{1}{\rho_k} \nu_k \cdot (A_k \nabla u_k) = -\frac{1}{\rho_j} \nu_j \cdot (A_j \nabla u_j) \qquad \text{on } \Sigma_{kj}, \tag{16}$$

$$\left(\frac{1}{\rho_k} \nu_k \cdot (A_k \nabla u_k) - i\varsigma u_k \right) = Q \left(-\frac{1}{\rho_k} \nu_k \cdot (A_k \nabla u_k) - i\varsigma u_k \right) + g \qquad \text{on } \Gamma_k, \tag{17}$$

where $u_k = u|_{\Omega_k}$, $Q \in \mathbb{C}$, $|Q| \leq 1$ and ς is a positive real valued on $\cup_{k=1}^K \partial\Omega_k$. We have also denoted $A_k = A|_{\Omega_k}$ and $\eta_k = \eta|_{\Omega_k}$. Note that A_k is either identity and $\eta_k = 1$ or the element is in the PML.

The boundary conditions (15) and (16) guarantee the continuity of the acoustic pressure

and normal particle velocity, respectively, across the element interfaces. The exterior boundary condition allows the implementation of various types of boundary conditions. For example, if $Q = 1$, equation (17) reduces to the Neumann type boundary condition $\nu_k \cdot (A_k \nabla u_k) = \frac{1}{2}\rho_k g$. Whereas $Q = -1$ produces the Dirichlet condition $u_k = \frac{i}{2\varsigma} g$. A source term can be implemented with the help of the functions f and g.

Following [2], the transmission conditions (15) and (16) on the interface Σ_{kj} may be written as impedance-like boundary conditions

$$\begin{aligned} \frac{1}{\rho_k}\nu_k \cdot (A_k \nabla u_k) - i\varsigma u_k &= -\frac{1}{\rho_j}\nu_j \cdot (A_j \nabla u_j) - i\varsigma u_j, \quad \text{and} \\ \frac{1}{\rho_k}\nu_k \cdot (A_k \nabla u_k) + i\varsigma u_k &= -\frac{1}{\rho_j}\nu_j \cdot (A_j \nabla u_j) + i\varsigma u_j. \end{aligned} \tag{18}$$

As proposed in [2] and used in previous UWVF studies [21], the coupling parameter ς is given as

$$\varsigma = \frac{1}{2}\left(\frac{\mathrm{Re}(\kappa_k)}{\rho_k} + \frac{\mathrm{Re}(\kappa_j)}{\rho_j}\right) \quad \text{on } \Sigma_{kj}. \tag{19}$$

This is the mean value of $\mathrm{Re}(\kappa)/\rho$ on the interface Σ_{kj}. On the exterior boundary Γ, the boundary parameter ς is chosen consistent with the exterior boundary condition. In all simulations of this study we use

$$\varsigma = \frac{\mathrm{Re}(\kappa_k)}{\rho_k} \quad \text{on } \Gamma_k. \tag{20}$$

Provided that $Q = 0$, $\kappa_k \in \mathbb{R}$, $A_k = I$, $g = 0$ and ς is given (20), the exterior boundary condition (17) corresponds to the zeroth order (i.e. Sommerfeld type) absorbing boundary condition

$$\frac{\partial u_k}{\partial \nu_k} - i\kappa_k u_k = 0 \quad \text{on } \Gamma_k. \tag{21}$$

This form is used in the numerical examples of Section 4 where the performance of the PML compared with the zeroth order absorbing boundary condition. Particularly, $A_k = I$ if we choose $\sigma_{0,\xi} = 0$, $\xi = x, y, z$.

For the formulation of the UWVF we define an operator

$$F_k : L^2(\partial\Omega_k) \to L^2(\partial\Omega_k) \tag{22}$$

such that if $y_k \in L^2(\partial\Omega_k)$ then $F_k(y_k) \in L^2(\partial\Omega_k)$ is given by

$$F_k(y_k) \quad = \quad \left(\frac{1}{\rho_k}\nu_k \cdot (\overline{A}_k\nabla) - i\varsigma\right) v_k \quad \text{on } \partial\Omega_k \tag{23}$$

where $v_k \in H^1(\Omega_k)$ satisfies

$$\nabla \cdot A_k\nabla\overline{v}_k + \kappa_k^2\eta_k^2\overline{v}_k = 0, \quad \text{in } \Omega_k, \tag{24}$$

and

$$\left(-\frac{1}{\rho_k}\nu_k \cdot (\overline{A}_k\nabla) - i\varsigma\right) v_k = y_k \text{ on } \partial\Omega_k. \tag{25}$$

In addition, we define the unknown impedance function χ_k on $\partial\Omega_k$ by

$$\chi_k = \Big(\big(-\frac{1}{\rho_k}\nu_k \cdot (A_k\nabla) - i\varsigma\big)u_k\Big)\Big|_{\partial\Omega_k}, \quad 1 \le k \le K. \tag{26}$$

Using integration by parts, the exterior boundary condition (17) and the coupled boundary conditions (18), the UWVF problem can be derived and is the problem of finding $\chi_k \in L^2(\partial\Omega_k),\ k = 1, 2, \ldots, K$ such that

$$\begin{aligned} &\sum_{k=1}^{K}\int_{\partial\Omega_k}\frac{1}{\varsigma}\chi_k\overline{y}_k - \sum_{k=1}^{K}\sum_{j=1}^{K}\int_{\Sigma_{kj}}\frac{1}{\varsigma}\chi_j\overline{F_k(y_k)} - \sum_{k=1}^{K}\int_{\Gamma_k}\frac{Q}{\varsigma}\chi_k\overline{F_k(y_k)} \\ = \quad &\sum_{k=1}^{K}\int_{\Gamma_k}\frac{1}{\varsigma}g\overline{F_k(y_k)} + \frac{2i}{\rho_k}\sum_{k=1}^{K}\int_{\Omega_k} f\eta_k^2\overline{v}_k \end{aligned} \tag{27}$$

for all $y_k \in L^2(\partial\Omega_k),\ k = 1, 2, \ldots K$. The derivation of (27) follows step by step the scheme developed by Cessenat and Després in [7].

3.1. Discretization

In order to discretize (27) we use a plane wave basis. We introduce a set of directions $\{a_{k,\ell}\}_{\ell=1}^{p_k}$ on Ω_k (with $|a_{k,\ell}| = 1$). Then the plane wave basis functions are

$$\varphi_{k,\ell} = e^{i\overline{\kappa}_k a_{k,\ell}\cdot\overline{r}'}. \tag{28}$$

where $\overline{r}' = (\overline{x}', \overline{y}', \overline{z}')$. Note that this special basis is a solution of the adjoint problem (14) on Ω_k when either $A_k = I$ or when we are in the PML. Similar plane wave basis functions have been used, for example, in the discontinuous Galerkin method for the 2D Helmholtz problem [13].

The discrete form of the UWVF is obtained via the substitution $v_k = \varphi_{k,\ell}$ and

$$\chi_k^a = \sum_{\ell=1}^{p_k} \Big(\chi_{k,\ell} \big(-\frac{1}{\rho_k} \nu_k \cdot (A_k \nabla) - i\varsigma \big) \varphi_{k,\ell} \Big), \quad 1 \le k \le K. \tag{29}$$

The unknown discrete impedances $\chi_{k,\ell}$ are computed from (27). Directions for the plane waves $a_{k,\ell}$ are chosen from optimized spherical coverings [18]. The number of directions per element is allowed to vary from 1 to 130. We shall describe shortly how the number is chosen.

Following [6] and [7], the discrete UWVF can be formulated as the matrix equation

$$(I - D^{-1}C)X = D^{-1}b \tag{30}$$

from which the weight vector $X = (\chi_{1,1}, ..., \chi_{1,p_1}, \chi_{2,1}, ...)^T$ can be resolved. Here D is the block diagonal matrix arising from the first term on the left hand side of (27). As proposed in [21], we employ the dynamic method for building the matrix D and choosing a stable number of basis functions p_k for each element. More precisely, the diagonal of the matrix D consists of K blocks D_k, i.e. one block per each element Ω_k. We choose the largest p_k for which the condition number of D_k is below a user specified limit. This preconditioning approach allows the use of a relatively simple bi-conjugate gradient iteration for solving (30) for the weight vector X.

It is noteworthy that the PML with the zeroth order damping coefficient ($n = 0$ in equations (2)-(3)), results in matrices D and C with entries that can be computed analytically whereas for higher order layers the integrals must be computed with a quadrature. Recalling that the integrands are severely oscillatory, the use of the quadrature increases dramatically the computational complexity of the UWVF-PML. In that case, it might be possible to develop a semi-analytical integration scheme, such as in [5], to speed up the integration. This topic, however, is not studied further here.

3.2. Resolving the field from the impedance data

The discrete UWVF gives an approximation to u and $\frac{\partial u}{\partial \nu}$ on $\partial\Omega_k$ for each k. However, away from $\partial\Omega_k$ a direct approximation is only given when there is no absorption in the problem. Since elements Ω_k are typically large compared to the wavelength of sound, we need to compute the field away from $\partial\Omega_k$ when medium is absorbing. We discuss a procedure to do this next.

Provided that A_k is identity matrix, $\kappa_k \in \mathbb{R}$ and $r' \in \mathbb{R}^3$ in Ω_k, equations (14) and (24) are identical. Therefore, it easily follows from (26) and (29) that

$$u^a|_{\Omega_k} = \sum_{\ell=1}^{p_k} \chi_{k,\ell}\varphi_{k,\ell}. \quad \text{in } \Omega_k. \tag{31}$$

In the case of absorbing medium, the extension of the field into the element requires a new post-processing step. (Note that this is not necessary during the solution of (30) but only for obtaining the field away from $\cup_{k=1}^{K}\partial\Omega_k$.)

Analogously with the original UWVF discretization (26) and (28), we utilize plane wave solutions to construct a new set basis functions. Unlike in the discrete UWVF, however, the plane waves are now solutions of the local Helmholtz equation (14) of the form

$$\phi_{k,\ell} = e^{i\kappa_k a_{k,\ell}\cdot r'}. \tag{32}$$

Rewriting the impedance equation (29) with the new set basis functions we obtain

$$\psi_k^a = \sum_{\ell=1}^{p_k} \Big(\psi_{k,\ell}\big(-\frac{1}{\rho_k}\nu_k\cdot(A_k\nabla) - i\varsigma\big)\phi_{k,\ell}\Big), \quad 1 \le k \le K. \tag{33}$$

To approximate the solution using the new basis, we need to compute the weights $\psi_{k,\ell}$, $1 \le \ell \le p_k$ for which $\psi_k^a \cong \chi_k^a$.

In the UWVF context, the weights can be easily obtained for each element $\Omega_k,\ 1 \le k \le K$ as a solution of

$$\begin{aligned}\sum_{\ell=1}^{p_k}\int_{\partial\Omega_k}\Big(\psi_{k,\ell}\big(-\frac{1}{\rho_k}\nu_k\cdot(A_k\nabla) - i\varsigma\big)\phi_{k,\ell}\Big)\overline{\Big(\big(-\frac{1}{\rho_k}\nu_k\cdot(\overline{A}_k\nabla) - i\varsigma\big)\phi_{k,m}\Big)}\\ = \sum_{\ell=1}^{p_k}\int_{\partial\Omega_k}\Big(\chi_{k,\ell}\big(-\frac{1}{\rho_k}\nu_k\cdot(A_k\nabla) - i\varsigma\big)\varphi_{k,\ell}\Big)\overline{\Big(\big(-\frac{1}{\rho_k}\nu_k\cdot(\overline{A}_k\nabla) - i\varsigma\big)\phi_{k,m}\Big)},\end{aligned} \tag{34}$$

for all $1 \le m \le p_k$. For each element, the equations (34) can be written in the form of matrix equation

$$Y_k = D_k^{-1}(\phi_{k,\ell},\phi_{k,m})D_k(\varphi_{k,\ell},\phi_{k,m})X_k \tag{35}$$

where $X_k = (\chi_{k,1},...,\chi_{k,p_k})^T$ and $Y_k = (\psi_{k,1},...,\psi_{k,p_k})^T$. The entries for the matrix D_k are

$$D_k(\phi_{k,\ell},\phi_{k,m}) = \int_{\partial\Omega_k}\Big(\big(-\frac{1}{\rho_k}\nu_k\cdot(A_k\nabla) - i\varsigma\big)\phi_{k,\ell}\Big)\overline{\Big(\big(-\frac{1}{\rho_k}\nu_k\cdot(\overline{A}_k\nabla) - i\varsigma\big)\phi_{k,m}\Big)}, \tag{36}$$

where $1 \leq \ell, m \leq p_k$. We note that in the case of $\kappa_k \in \mathbb{R}$ and $r' \in \mathbb{R}^3$ in Ω_k, the term $D_k^{-1}(\phi_{k,\ell}, \phi_{k,m}) D_k(\varphi_{k,\ell}, \phi_{k,m}) = I$ and no post-processing is needed.

After the coefficients $\psi_{k,\ell}$ are found, the approximation for the field in each element is obtained as

$$u^a|_{\Omega_k} = \sum_{\ell=1}^{p_k} \psi_{k,\ell} \phi_{k,\ell} \quad \text{in } \Omega_k. \tag{37}$$

4. Numerical studies

To investigate the feasibility of the UWVF-PML method for large-scale wave field simulations, we now perform a series of numerical experiments concerned with the propagation and scattering of time-harmonic acoustic waves. It is known from experience with finite difference and finite element methods that the PML parameters n, $\sigma_{0,\xi}$ and the thickness of the PML must be properly adjusted to reduce numerical reflections to an acceptable level. We analyze the effect of the PML-parameters to the accuracy of the UWVF-PML approximation. Since in the simulations, the decay parameter $\sigma_{0,\xi}$, $\xi = x, y, z$ has identical growth rate with respect to all directions x, y and z, we denote it simply by $\sigma_0 = \sigma_{0,\xi}$. Relative errors presented in the following sections are computed using the discrete L^2-norm.

As noted in Section 3.1, the directions for the plane wave basis functions are obtained from optimized spherical coverings [18]. The number of basis functions for each element is chosen based on the condition number of the matrix block D_k [21]. The maximum allowed condition number in all simulations is set to 10^6. According to our experience, when the element size of the mesh is not very large compared to the wavelength (e.g. $\lambda/h < 0.3$ in this study) this choice provides an accuracy which is limited by the spurious boundary reflections. However, as was shown in [21], the condition number limit must be set higher for coarser meshes in order to maintain the same level of accuracy.

The number of basis functions per element in our code is limited to between 1 and 130. The element size is chosen so that the upper limit for the number of basis functions is not exceeded. More precisely, at most 92 basis functions per element is needed in the simulations of this study. The discrete problem (30) is solved by the stabilized bi-conjugate gradient iteration

which is truncated when the relative residual reaches a value below 10^{-6}. Typically 100-300 iterations are required to reach the termination criterion.

The computer code used in this study is written in Fortran90 and parallelized using MPI (Message Passing Interface). The computations are done with Beowulf PC clusters consisting of either 11 1.8 GHz Pentium 4 processors and having 11.5 GB total RAM; or 24 2.6 GHz Pentium 4 processors and having 48.0 GB total RAM.

4.1. A point source

The first test problem consists of a point source

$$u(r, r_0) = \frac{1}{4\pi} \frac{e^{i\kappa|r-r_0|}}{|r-r_0|} \tag{38}$$

in a cubic computational domain centered at the origin. The location of the source is off-centered at $r_0 = (10, 10, 10)$ mm and $r = (x, y, z)$ is an observation point. The domain consist of two concentric cubes with side lengths 30 and 40 mm. The region outside the smaller cube constitutes the PML (see Fig. 2).

In all examples for this model problem we have set $c = 1500$ m/s, $\rho = 1000$ kg/m^3 and $\omega = 2\pi \cdot 500$ kHz. Hence, the wavelength is $\lambda = 3.0$ mm. Fig. 2 also shows a cross-section of a typical mesh used in simulations. The longest edge of a tetrahedron in that mesh is $h = 7.2$ mm which is over twice the wavelength. In terms of wavelengths, the size of the non-PML region is $10 \times 10 \times 10$ wavelengths.

The PML is chosen to be $1\frac{2}{3}$ wavelengths thick and consists of 1-2 layers of elements. The thickness of the layer is similar to that used in FDTD studies [3], but in the FDTD method it is usual to have 8-10 elements in the layer. In contrast the UWVF allows larger elements having multiple degrees of freedom per element,

In the UWWF, a point source is obtained by setting $g = 0$ and $f = \delta(r - r_0)$ in (14)- (17) where $\delta(r - r_0)$ is the Dirac delta function. The right hand side for Equations (27) and (30) is thus

$$b_{k,\ell} = \frac{2i}{\rho_k} \sum_{k=1}^{K} \int_{\Omega_k} f\overline{\varphi}_k = \frac{2i}{\rho_k} e^{-i\overline{\kappa}_k a_{k,\ell} \cdot r_0} \tag{39}$$

[Figure 2 about here.]

[Figure 3 about here.]

The UWVF-PML approximations are computed for the zeroth order damping layer (i.e. $n = 0$) and by varying the damping coefficient $\sigma_{0,\xi} = \sigma_0$. We note that the decay function σ_ξ is of the form $\sigma_\xi(\xi) = \sigma_0(|\xi| - \xi_0)^n, \quad \xi = x, y, z$ where $|\xi| - \xi_0$ in this study is typically 0.005 m. This necessitates a quite large value of the parameter σ_0.

For the exterior boundary condition (17), we have set $Q = 0$, $g = 0$ and the parameter ς is given in (20). We note that in the case of $\sigma_0 = 0$, the exterior boundary condition corresponds to the zeroth order absorbing boundary condition (21). The exact solution and UWVF-PML approximations with different σ_0 are shown in Fig. 3. Relative errors in the $x = 0$ mm plane inside the inner cube are listed in Table I. We list also the variation in the number of basis function per element p_k, the number of degrees of freedom in the problem (DOF) and variation in parameter $\sqrt[3]{6p_k}\frac{\lambda}{h_k}$ where h_k is the longest edge of the tetrahedron Ω_k. This parameter can be considered as an indicator to the needed number of degrees of freedom per wavelength. The UWVF uses values $\sqrt[3]{6p_k}\frac{\lambda}{h_k} < 6.7$ that are below the rule of thumb $\frac{\lambda}{h} \approx 10$ typical for low order finite elements. Despite that the error of the UWVF-PML approximations is below 1 %.

[Table 1 about here.]

The same mesh (Fig. 2) is used in all the simulations reported in Table I. It consists of 2 558 vertices and 12 521 tetrahedra. However, since the number of plane wave basis functions in each element Ω_k is chosen according to the condition number of the corresponding matrix block D_k, the choice of the decay parameter σ_0 affects the number of basis functions in the PML elements.

The smallest errors occurs with the value $\sigma_0 = 500$. A larger σ_0 results in a slightly poorer accuracy. This is most likely due to the conditioning based method for choosing the number of basis functions for each element. More precisely, increasing σ_0 deteriorates the conditioning of the matrix blocks D_k and thus reduces the number of basis functions per element. The

smaller number of plane wave basis functions weakens the matching of the UWVF impedance functions across elements faces and naturally increases the error. On the other hand, for the lower σ_0 the reduced number of basis functions in the PML decreases the number of degrees of freedom for the problem while σ_0 is large enough that high accuracy still remains. A plot along y-axis shows the rapid decay of the field in the PML (Fig. 4).

[Figure 4 about here.]

To investigate the higher order PML (i.e. $n > 0$), we show two $n = 2$ examples with $\sigma_0 = 6 \cdot 10^7$ and $\sigma_0 = 8 \cdot 10^7$ in Fig. 5. The values of σ_0 are chosen so that the integrals of the stretched variables (2)-(4) are comparable with the best performing $n = 0$ examples. The errors for $\sigma_0 = 6 \cdot 10^7$ and $\sigma_0 = 8 \cdot 10^7$ are 1.76 % and 0.62 %, respectively. In the same problem, the error for $n = 0$ and $\sigma_0 = 500$ is 0.38 % which is slightly smaller than obtained with the higher order $n = 2$ layer. In addition, note that the disadvantage of using $n > 0$ is a much greater time for matrix assembly without a marked improvement in accuracy.

[Figure 5 about here.]

Results of Table I show that compared to the Sommerfeld-type ABC ($\sigma_0 = 0$), the PML reduces the error. However, the Sommerfeld-type condition becomes more accurate if the absorbing boundary is moved farther from the point source. Then, a question arises whether it is more efficient to use the PML than the ABC to obtain a desired level of accuracy. This is examined next by using the same test with the point source at $(10, 10, 10)$ mm as in the previous paragraphs.

The efficiency of the PML method is compared with the zeroth order absorbing boundary condition in Table II. The PML0 example with $n = 0$ and $\sigma_0 = 500$ is the same as in Table I; and Figs. 3 and 4. The second order PML (PML2 in the table) corresponds to the case $n = 2$ and $\sigma_0 = 8 \cdot 10^7$ in Fig. 5. To reduce the error, the size of the computational domain in the case of the Sommerfeld-type condition is $70 \times 70 \times 70$ mm. In the table we list, for example, the number of stabilized bi-conjugate gradient iterations (Iter), the memory requirement in gigabytes (Mem) and the total computation time t using a Beowulf PC cluster with 24 2.6 GHz Pentium 4 processors and 48.0 GB total RAM.

[Table 2 about here.]

Despite the larger computational domain, and therefore increased memory need and CPU time, the accuracy of the zeroth order ABC remains lower than the accuracy of the PML method. The error of the second order PML is comparable with the $n = 0$ case but the computation time is huge due to the numerical integration needed in the matrix assembly.

We also studied the error of UWVF-PML approximations as a function of the source - PML separation. For this experiment the point source (38) is located at the origin ($r_0 = (0, 0, 0)$) and the PML is defined between two concentric cubes as in Fig. 2. The side length of the non-PML domain varies from 4 to 25 mm. The thickness of the PML in all simulation is 5 mm. Figure 6 plots errors using the PML parameters $\sigma_0 = 0$ and $\sigma_0 = 500$ in the case of $n = 0$. All errors are computed in the 1.9×1.9 mm region in the $x = 1.9$ mm plane.

[Figure 6 about here.]

The accuracy with $\sigma_0 = 500$ remains somewhat independent of the nearness of the PML while the error for $\sigma_0 = 0$ decreases with the distance of the exterior boundary. A reason for the unevenness of the error maybe a variation in the mesh quality. We note that the meshes in the case of $\sigma_0 = 0$ and $\sigma_0 = 500$ are identical for a fixed size of the computational domain, however, the number of basis functions in the PML elements varies. Since the thickness of the PML (5 mm) corresponds to almost two wavelengths, the zeroth order ABC (i.e. $\sigma_0 = 0$) performs relatively well.

The overall errors in the case of $\sigma_0 = 0$ are smaller than in the first test problem (Table I). This is due to the location of source at the origin. Namely, waves hit the exterior boundary at relatively small angles resulting in diminished numerical reflections from the absorbing boundary condition (21). On the other hand, the field inside the computational domain is more symmetric than in the case of off-centered source. This may also reduce the effect of spurious reflections.

4.2. Inhomogeneous and absorbing medium

For the second example we divide the computational domain into two parts with the plane $z = 0$. The material properties for the upper ($z > 0$) and lower ($z < 0$) half spaces are (κ_1, ρ_1) and (κ_2, ρ_2), respectively. We use complex wave numbers κ_1 and κ_2, i.e. the materials have non-zero absorption coefficients $\alpha_1 = 20$ Np/m and $\alpha_2 = 40$ Np/m. The other material parameters are $c_1 = 1500$ m/s, $c_2 = 2000$ m/s, $\rho_1 = 1000$ kg/m^3 and $\rho_2 = 1200$ kg/m^3. These result in wavelengths $\lambda_1 = 3$ mm and $\lambda_2 = 4$ mm for upper and lower half spaces.

As in the first example, the field is emitted by a point source located at the point $(0, 0, h)$ where $h = 10$ mm. An analytical solution for the field is [11]

$$u(r,h) = \begin{cases} \dfrac{e^{i\kappa_1 R^+}}{4\pi R^+} + \dfrac{e^{i\kappa_1 R^-}}{4\pi R^-} - \dfrac{\beta}{2\pi}\displaystyle\int_0^\infty J_0(\zeta R) e^{-\mu_1(z+h)} \frac{\zeta \mu_2 d\zeta}{\mu_1(\beta\mu_2 + \mu_1)}, & z > 0 \\ \dfrac{1}{2\pi}\displaystyle\int_0^\infty J_0(\zeta R) e^{\mu_2 z - \mu_1 h} \frac{\zeta d\zeta}{\beta\mu_2 + \mu_1}, & z < 0 \end{cases} \tag{40}$$

where $R = \sqrt{x^2 + y^2}$, $R^\pm = \sqrt{R^2 + (z \mp h)^2}$ and $\beta = \rho_2/\rho_1$. The Bessel function of order zero is denoted by J_0 and $\mu_j = \sqrt{\lambda^2 - \kappa_j^2}$, $j = 1, 2$. The integrals of (40) can be easily approximated with the trapezoidal rule. Since integrands of (40) decay rapidly, the upper bound of the integral can be chosen so that no significant truncation errors occur from replacing the infinite limit by a finite value.

As discussed in Section 3.2, equation (31) should not be applicable to approximate the field inside elements where the wave number is complex and an additional post-processing step is required. Since Equation (31) remains valid on the element interfaces $\partial\Omega_k$, it is useful to estimate the error that follows from the use of (31) for the elements in the absorbing media. Therefore, we compare in Table III the accuracy of the fields computed using (31) and (37). The corresponding UWVF approximations and the exact solution for the problem are presented in Fig. 7. It is clear that the use of (37) improves the accuracy of the scheme.

[Table 3 about here.]

[Figure 7 about here.]

4.3. Uniformly oscillating surface on a rigid baffle

The third test problem is typical for many applications of acoustics. We study a field generated by a rigid infinite surface of which a finite region S is oscillating with normal velocity amplitude v_n. The field generated by such a source in a homogeneous fluid can be computed using the Rayleigh integral

$$u = \frac{i\kappa\rho v_n}{2\pi}\int_S \frac{e^{i\kappa|r-r_0|}}{|r-r_0|}dS(r_0), \tag{41}$$

where we now denote by r_0 a point on the oscillating surface. In addition, we assume that the velocity amplitude v_n is uniform throughout the surface S. The region of interest has dimensions $30 \times 95 \times 30$ mm which is surrounded by a 5 mm thick damping layer (see Fig. 8). We use the zeroth order PML ($n = 0$). Although the optimal value of the damping parameter σ_0 is case dependent [9], from the point of view stability and accuracy, the numerical simulations of Sections 4.1 and 4.2 suggest that σ_0 should be as high as possible but not too high which may deteriorate the conditioning of the problem. This argument motivates us to choose $\sigma_0 = 500$.

The material parameters for the medium are identical to those for the first test problem. The angular frequency used in this problem is $\omega = 2\pi \cdot 500$ kHz. Hence, the wavelength is $\lambda = 3$ mm and the size of the non-PML region is $10 \times 31\frac{2}{3} \times 10$ wavelengths.

The oscillating and rigid boundaries are obtained using Neumann type boundary conditions in the UWVF. More precisely, in the $y = 0$ plane, we choose $Q = 1$, $f = 0$ and ς as in (20). In addition, we set $g = -2i\omega v_n$ and $g = 0$ for the oscillating and rigid boundaries, respectively. The rectangular face in the $y = 0$ plane with the side length of 20 mm acts as the source while the rest of the plane is modeled as a rigid surface (see Fig. 8).

The fields are presented in Fig. 9. Use of the PML reduces the error from 8.18% to 1.54% compared to the case $\sigma_0 = 0$ which corresponds the zeroth order ABC. The variability in the number of basis functions per element was 42-85 for $\sigma_0 = 0$ and 10-84 when $\sigma_0 = 500$. The benefit of the damping layer can be seen more clearly on the central axis of the source (Fig.10).

[Figure 8 about here.]

[Figure 9 about here.]

[Figure 10 about here.]

5. Discussion

We have studied the feasibility of the perfectly matched layer absorbing boundary condition for the three dimensional ultra weak variational formulation of the Helmholtz equation. The PML was derived using complex stretching of spatial variables. This led to the modified Helmholtz equation for which the UWVF was formulated.

The suitability of the method for the large-scale numerical modeling of acoustic fields was investigated with computational experiments. In comparison with a low order absorbing boundary condition, the zeroth order ($n = 0$) PML showed significant improvement in accuracy. In all problems studied, the accuracy of the UWVF-PML approximation could be adjusted to obtain an error of the order 1 %. Which is sufficient accuracy for most engineering applications. We also studied higher order PML (i.e. $n > 0$). However, for the model problems of this study, this did not cause an improvement in accuracy. Instead, the building of the UWVF matrices required numerical integration which dramatically increased the computational burden.

It is notable that the thickness of the PML in the simulations of this study is relatively large. One might expect that this results in an unnecessarily large storage requirement. However, due to the relatively small number of basis functions per element in the PML, the storage for PML elements is smaller than for the elements in the non-PML region. This also explains the reduction in the number of degrees of freedom with the increase of the decay parameter σ_0, see Table I. On the other hand, since the PML consist of 1-2 layers of elements, a thinner PML might lead to smaller elements near the edge of the non-PML region which might not reduce the over-all storage requirement of the problem. This is because, at least in 2D, it is beneficial to use as large elements as possible and a large number of basis functions per elements [21].

Compared to a low order finite element method (FEM), numerical studies in 2D suggest that the UWVF method reduces the overall storage needed for a problem [20]. It is likely that the number of degrees of freedom in the 3D UWVF is also lower than needed for the

FEM. However, a rigorous assessment of the UWVF compared to other 3D method remains to be done. A drawback of the UWVF method is the difficulty of finding the right number of plane basis functions for each element. Namely, the computation time needed for assembling the matrix D and choosing the number of plane waves for each element is strongly dependent on the initial guess of the number of directions p_k. In a typical simulation of this study, the building of the matrix D took over a half of the total CPU time.

Another drawback of the UWVF method is its limitation to the piecewise constant material properties. More precisely, the density of the medium and wave number must be constant in a single element. This limits the feasibility of the method for problems in which these parameters are smooth functions of position. However, a method for constructing 2D plane wave basis functions for linearly varying material parameters has been developed in [4]. A similar technique may be possible also with the 3D UWVF method.

Although this study is dedicated to studying the performance of the perfectly matched layer, it is interesting to investigate alternative methods for reducing numerical reflections. In this regard an important family of boundary conditions are the Higdon-type conditions [19] which are exact for plane waves propagating to known directions and may therefore be effective with the UWVF method which uses plane wave basis functions. On the other hand, other high-order methods, such as discussed in [1, 16], may improve the accuracy of the UWVF method.

The directions for the plane wave basis functions in the UWVF were uniformly distributed on the unit sphere and the number of directions per element were chosen according to a conditioning based criterion. The maximum allowed condition number for the matrix blocks D_k in all simulations was set to 10^6. Using this scheme, the accuracy of the UWVF approximation in all numerical examples was mainly limited by the absorbing boundary condition. However, when the PML parameter σ_0 was chosen very high, it resulted in an insufficient number of basis functions for PML elements, decreasing the accuracy of the UWVF approximation.

Since directions for the basis functions were distributed uniformly on the unit sphere, they did not include any a priori information about the direction of propagation of the field to be solved. It is obvious that if the directions could be matched a priori with the solution field, a significant reduction in the number of basis functions needed would occur. In a finite element

scheme, this kind of approach has been implemented using a ray method for determining the optimized directions [14]. Another alternative is to use an adaptive method, such as discussed in [23]. We are now considering such an approach.

REFERENCES

1. A. Bayliss, M. Gunzburger, and E. Turkel. Boundary conditions for the numerical solution of elliptic equations in exterior regions. *SIAM Journal of Applied Mathematics*, 42(2):430–451, 1982.
2. J.D. Benamou and B. Després. A domain decomposition method for the Helmholtz equation and related optimal control problems. *Journal of Computational Physics*, 136:68–82, 1997.
3. J. Berenger. A perfectly matched layer for the absorption of electromagnetic waves. *Journal of Computational Physics*, 114:185–200, 1994.
4. P. Bettess. Special wave basis finite elements for very short wave refraction and scattering problems. *Communications in Numerical Methods in Engineering*, 20(4):291–298, 2004.
5. P. Bettess, J. Shirron, O. Laghrouche, B. Peseux, R. Sugimoto, and J. Trevelyan. A numerical integration scheme for special finite elements for the Helmholtz equation. *International Journal for Numerical Methods in Engineering*, 56(4):531–552, 2003.
6. O. Cessenat. *Application d'une nouvelle formulation variationelle des equations d'ondes harmonigues, Problemes de Helmholtz 2D et de Maxwell 3D.* PhD thesis, Paris IX Dauphine, 1996.
7. O. Cessenat and B. Després. Application of an ultra weak variational formulation of elliptic PDEs to the two-dimensional Helmholtz problem. *SIAM Journal of Numerical Analysis*, 35(1):255–299, 1998.
8. W.C. Chew and W.H. Weedon. A 3D perfectly matched medium from modified Maxwell's equations with stretched coordinates. *Microwave and Optical Technology Letters*, 7(13):599–604, 1994.
9. F. Collino and P. Monk. Optimizing the perfectly matched layer. *Computer Methods in Applied Mechanics and Engineering*, 164:157–171, 1998.
10. F. Collino and P. Monk. The perfectly matched layers in curvilinear coordinates. *SIAM Journal of Scientific Computing*, 19(6):2061–2090, 1998.
11. D. Colton and P. Monk. Mathematical and numerical methods in inverse acoustic scattering theory. *Zeitschrift für Angewandte Mathematik und Physic*, 81(723-731), 2001.
12. B. Engquist and A. Majda. Absorbing boundary conditions for the numerical simulation of waves. *Mathematics of Computation*, 31(139):629–651, 1977.
13. C. Farhat, I. Harari, and U. Hetmaniuk. A discontinuous Galerkin method with Lagrange multipliers for the solution of Helmholtz problems in the mid-frequency regime. *Computer Methods in Applied Mechanics and Engineering*, 192:1389–1419, 2003.
14. E. Giladi and J. B. Keller. A hybrid numerical asymptotic method for scattering problems. *Journal of Computational Physics*, 174(1):226–247, 2001.
15. D. Givoli. Non-reflecting boundary conditions. *Journal of Computational Physics*, 94:1–29, 1991.

16. M.J. Grote and J.B. Keller. On nonreflecting boundary conditions. *Journal of Computational Physics*, 122:231–243, 1995.
17. I. Harari, M. Slavutin, and E. Turkel. Analytical and numerical studies of a finite element PML for the Helmholtz equation. *Journal of Computational Acoustics*, 8(1):121–137, 2000.
18. R.H. Hardin, N.J.A. Sloane, and W. D. Smith. Spherical coverings. Electronic: http://www.research.att.com/ njas/coverings/index.html, May 1997.
19. R.L. Higdon. Absorbing boundary conditions for difference approximations to the multi-dimensional wave equation. *Mathematics of Computation*, 47(176):437–459, 1986.
20. T. Huttunen, P. Monk, F. Collino, and J.P. Kaipio. The ultra weak variational formulation for elastic wave problems. *SIAM Journal on Scientific Computing*, 2003. Accepted.
21. T. Huttunen, P. Monk, and J.P. Kaipio. Computational aspects of the ultra-weak variational formulation. *Journal of Computational Physics*, 182:27–46, 2002.
22. J.B. Keller and D. Givoli. Exact non-reflecting boundary conditions. *Journal of Computational Physics*, 82:172–192, 1989.
23. O. Laghrouche and P. Bettess. *Short wave modelling using special finite elements - Towards an adaptive approach*, chapter 10, pages 181–194. Mathematics of Finite Elements and Applications (MAFELAP 1999). Elsevier, 1999.
24. Q. Qi and T.L. Geers. Evaluation of the perfectly matched layer for computational acoustics. *Journal of Computational Physics*, 139:166–183, 1998.

List of Figures

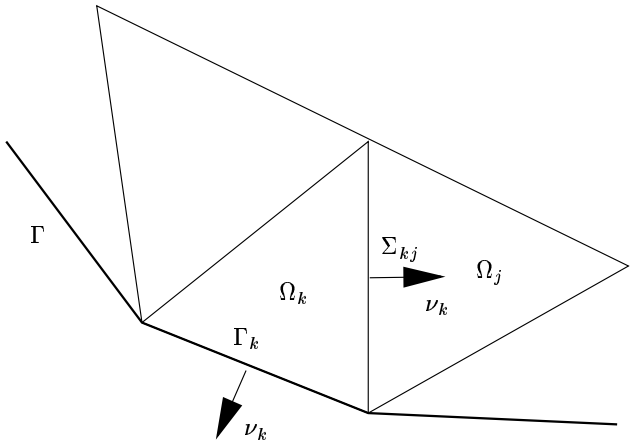

Figure 1. Notation for the finite element partition of the domain Ω. The edge Σ_{kj} separates elements Ω_k and Ω_j with outward normal ν_k. Boundary edges of Ω_k lying on the exterior boundary Γ are denoted Γ_k.

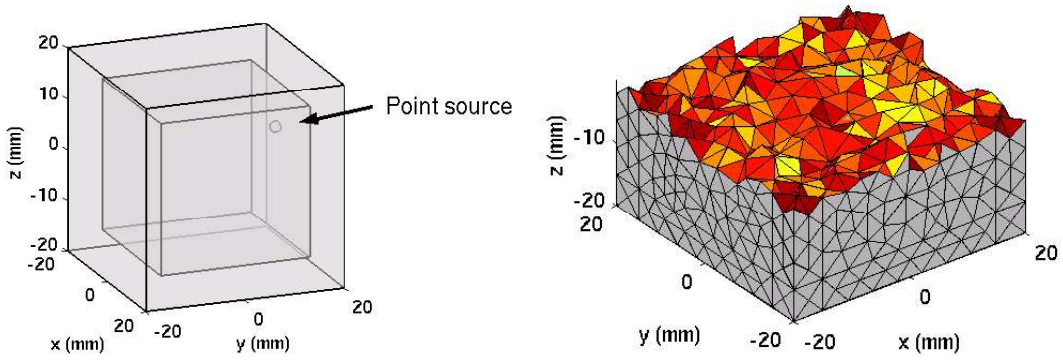

Figure 2. Geometry and a cross-section of the mesh for the model problem 1. A point source is located at $r_0 = (10, 10, 10)$ mm.

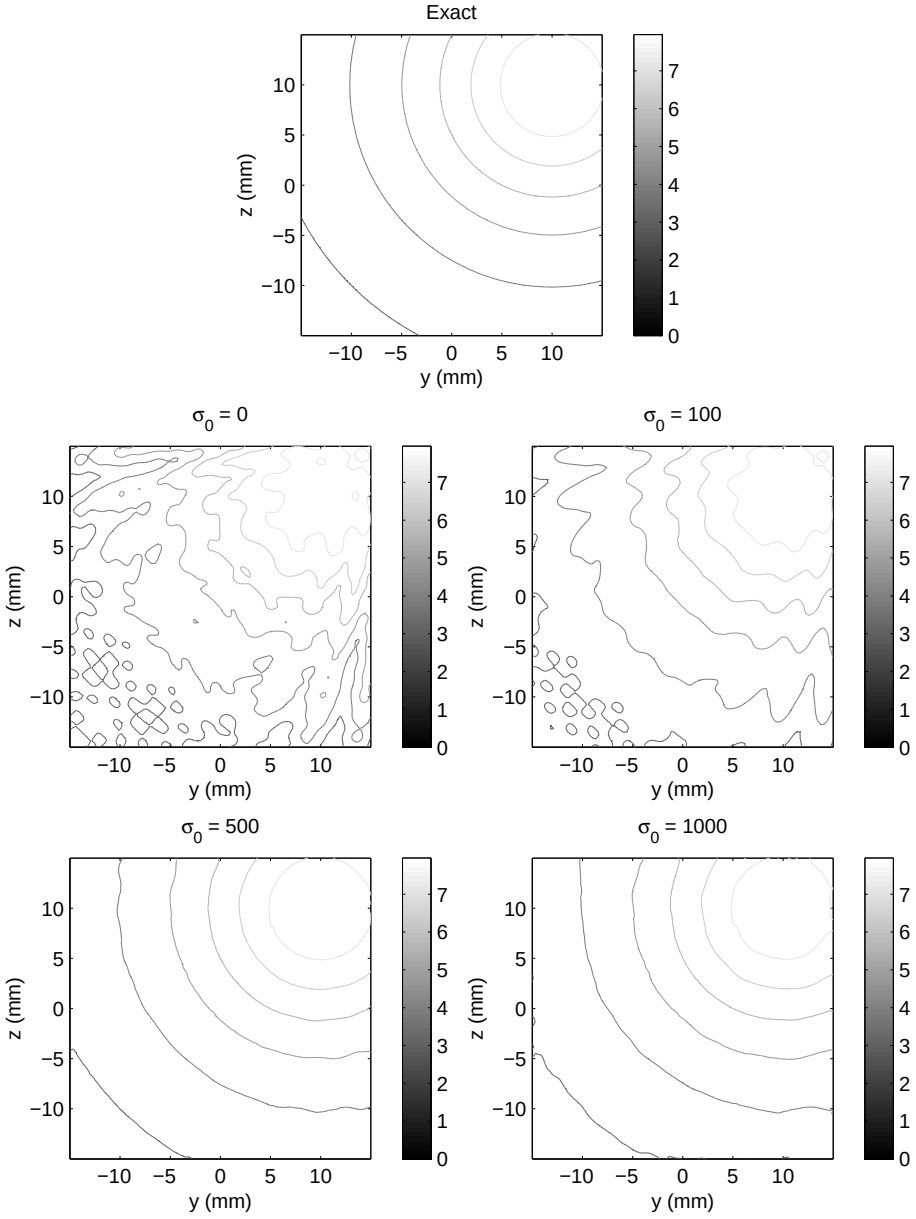

Figure 3. The absolute value of the exact field in the plane $x = 0$ (top row). The UWVF approximation with a zeroth order ($n = 0$) PML having different damping coefficients $\sigma_{0,\xi} = \sigma_0$ are shown in the remaining panels. Note that the field is shown in the non-PML region. The boundary condition (21) is used on the exterior boundary.

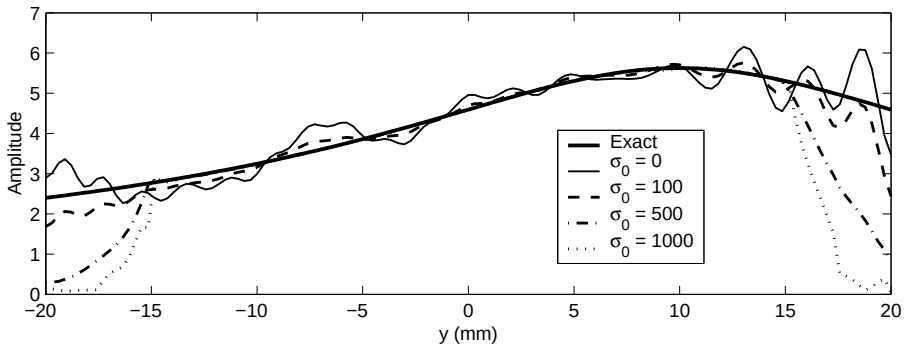

Figure 4. The amplitude of the acoustic field as a function of y for various damping parameter values. The fields along the y-axis decay inside the PML damping layer $|y| > 15$ mm. Outside the PML the field computed using $\sigma_0 = 500$ is indistinguishable from the exact solution. For a large damping coefficient, the adaptive choice of the plane wave basis functions in the UWVF allows only a small number directions for the elements in the PML. This is most likely a reason for the slightly reduced accuracy of UWVF approximation in the case of the largest σ_0.

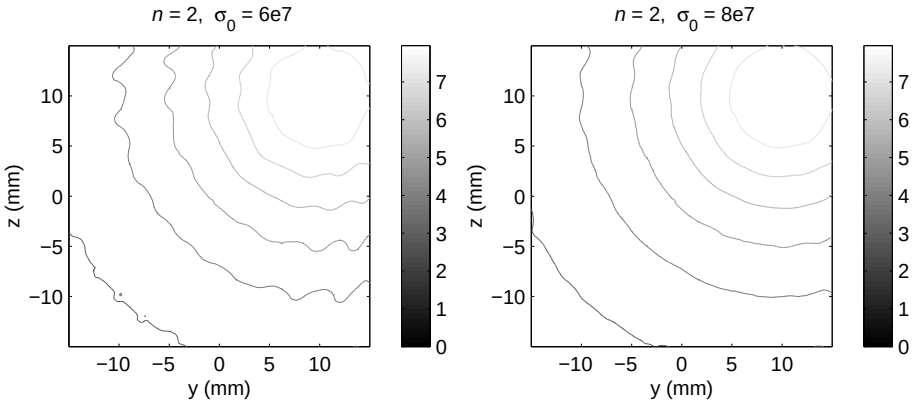

Figure 5. Two UWVF approximations with the second order ($n = 2$) PML with different damping coefficients $\sigma_{0,\xi} = \sigma_0$. Figures show the field inside the non-PML region in the $x = 0$ plane. The results are agreeable to the $n = 0$ case when $\sigma_0 = 500$ but take longer to compute.

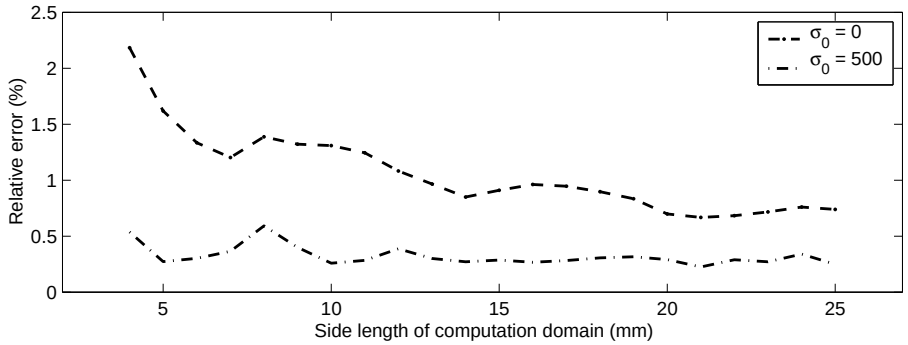

Figure 6. The error of the UWVF-PML with $n = 0$ as a function of side length of the non-PML region which measures the source-PML separation. The side length of the computational domain is for the cube forming the non-PML region. For this example there is little need to have the PML far from the source, but the accuracy of the zeroth order absorbing boundary condition (i.e. $\sigma_0 = 0$) is markedly degraded if the absorbing boundary is placed too close to the source.

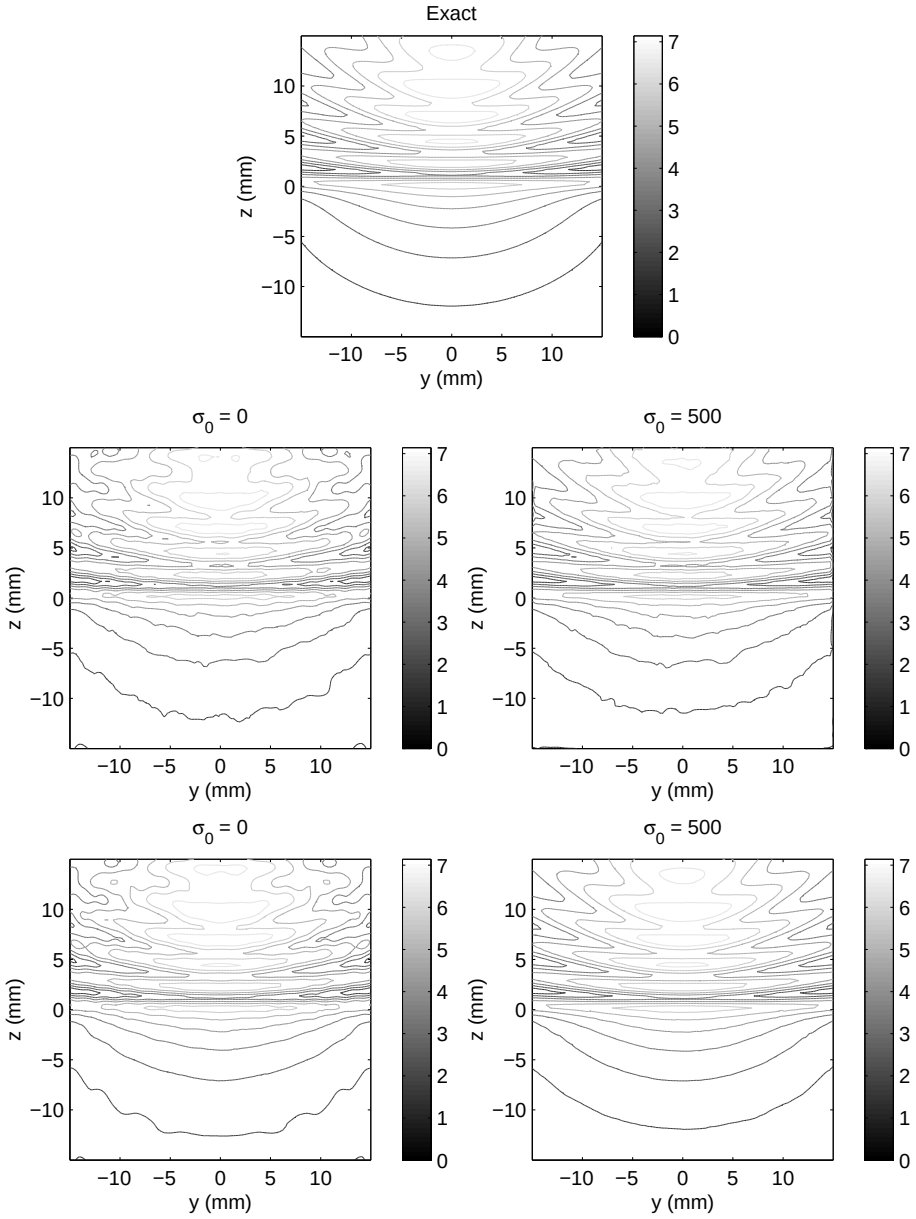

Figure 7. The exact solution (top row), the UWVF approximations when computed with equation (31) (middle row) and the UWVF approximations using Equation (37). Figures show the field inside the non-PML region in the $x = 10$ mm plane.

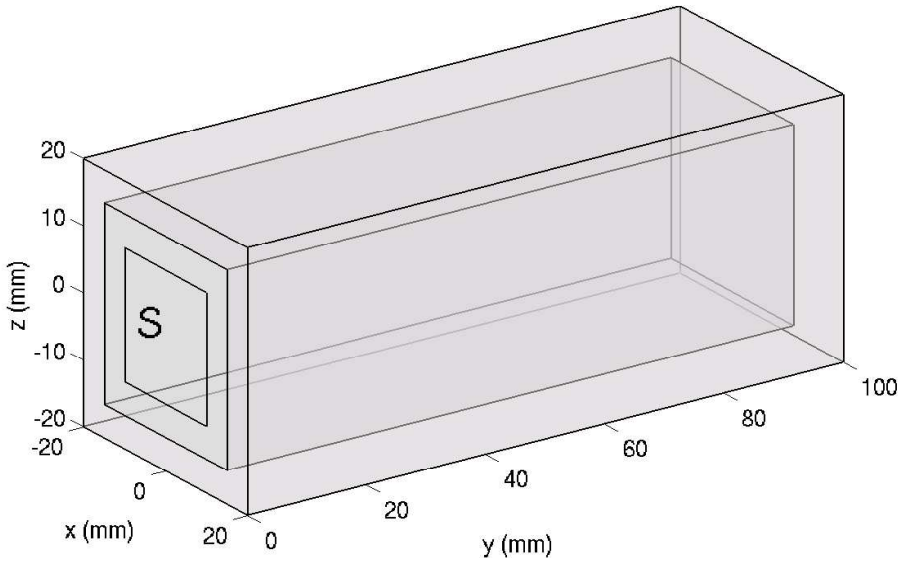

Figure 8. Geometry of the third model problem. The field is generated by a uniformly oscillating rigid surface S in the plate $y = 0$. The rest of the $y = 0$ face is modeled as a perfectly rigid surface. The region between the inner and outer cubes constitutes the PML.

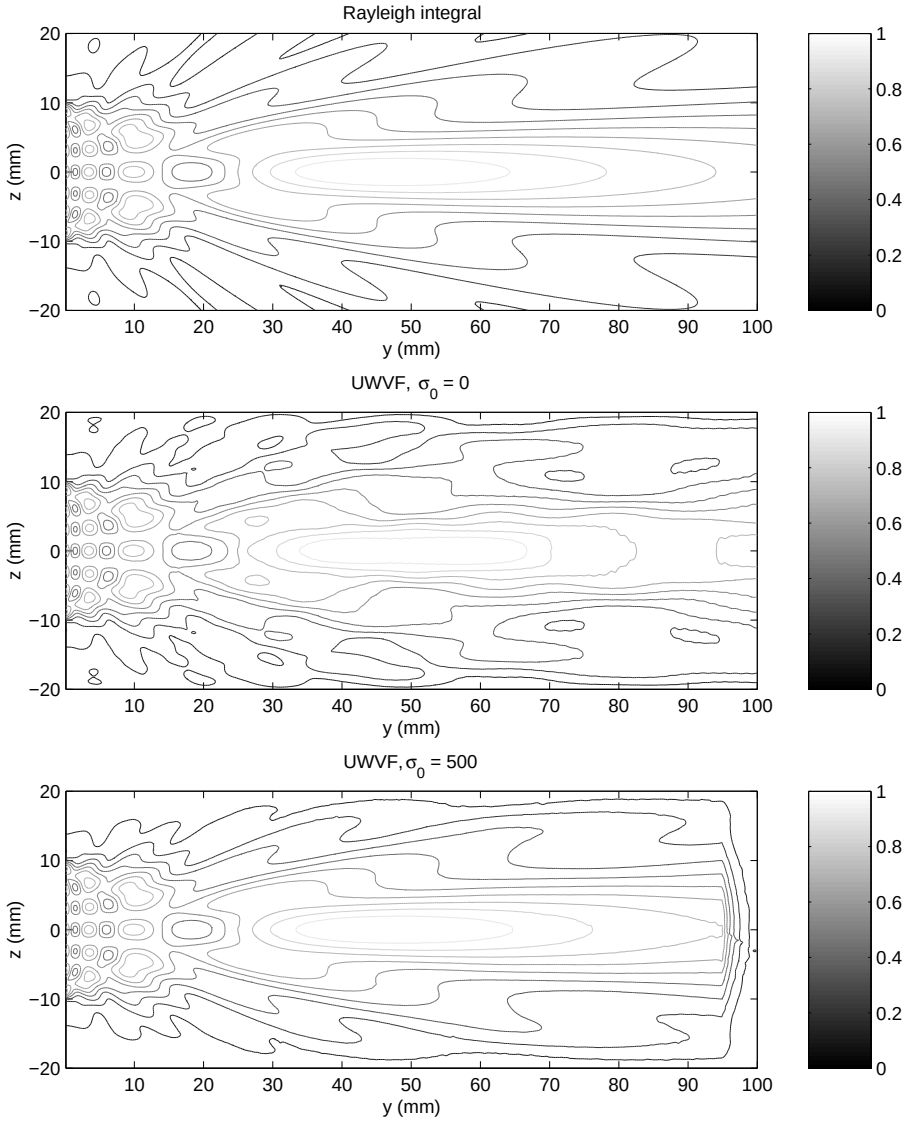

Figure 9. Rayleigh integral (top), the UWVF-PML approximation with $\sigma = 0$ (middle) and with $\sigma_0 = 500$ (bottom). The case of $\sigma_0 = 0$ corresponds to the zeroth order absorbing boundary condition (21). The PML starts when $|z| = 15$ mm and when $y = 95$ mm.

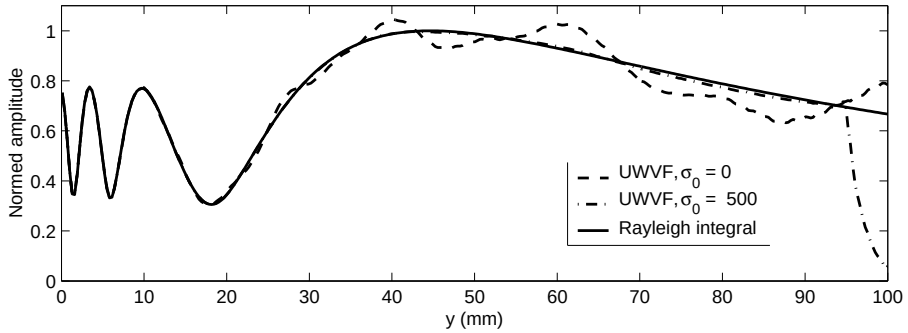

Figure 10. Comparison of the Rayleigh integral, the UWVF-PML with $\sigma_0 = 0$ and with $\sigma_0 = 500$ on the central axis of the source. The region $y > 95$ mm constitutes the PML.

List of Tables

Table I. Summary of the results of point source simulations

σ_0	p_k	DOF	$\sqrt[3]{6p_k}\frac{\lambda}{h_k}$	Err%
0	40 - 84	707 744	3.22 - 6.62	9.95
100	37 - 84	669 306	3.22 - 6.42	4.55
500	10 - 84	549 029	2.35 - 6.28	0.38
1000	1 - 84	422 666	1.09 - 6.28	0.62

Table II. Comparison of the PML and the zeroth order absorbing condition. PML0 corresponds to the parameters $n = 0$ and $\sigma_0 = 500$; and PML2 the parameters $n = 2$ and $\sigma_0 = 8 \cdot 10^7$.

Method	Domain (mm^3)	p_k	DOF	Iter	Mem (GB)	t(s)	Err%
PML0	$50 \times 50 \times 50$	10 - 84	549 029	140	3.9	399	0.38
PML2	$50 \times 50 \times 50$	9 - 84	580 103	868	4.2	13 323	0.62
Sommerfeld	$70 \times 70 \times 70$	46 - 92	2 918 501	216	19.0	1088	2.31

Table III. Simulations for inhomogeneous absorbing medium

Approximating Eq.	σ_0	Err%
(31)	0	5.54
	500	3.37
(37)	0	4.51
	500	0.41